Progress In Electromagnetics Research, Vol. 160, 51–61, 2017

Patch Antenna Using Rectangular Centre Slot and Circular Ground Slot for Circularly Polarized Synthetic Aperture Radar (CP-SAR) Application

Farohaji Kurniawan[1, 2, *], Josaphat T. Sri Sumantyo[1], Koichi Ito[3], Hiroaki Kuze[1], and Steven Gao[4]

Abstract—In this paper, a circularly polarized antenna for Synthetic Aperture Radar (SAR) application is presented. The antenna is proposed to be implemented for the airborne SAR and the spaceborne SAR. To enhance the bandwidth of the antenna, the Circular-Ring-Slot (CRS) technique is implemented on the ground plane and in a square slot in the centre of the patch. In this antenna's design, the model of the slot on the radiator is also investigated. The antenna is printed on NPC-H220A substrates with the dielectric constant of 2.17 and thickness of 1.6 mm. The resonant frequency of the antenna design sets at 9.4 GHz with the minimum requirement of the bandwidth of 800 MHz. The antenna design is produced under the −10 dB bandwidth of reflection coefficient, S_{11} of approximately 27% (8.2 GHz–10.76 GHz) and left-handed circular polarization (LHCP). The gain of the antenna is 6.5 dBic and 12.7% (8.8 GHz–9.84 GHz) for the axial ratio bandwidth (ARBW). This paper includes the description and presentation of the completed discussion.

1. INTRODUCTION

Nowadays, the Synthetic Aperture Radar (SAR) attracts the interest of many researchers regarding to its advantages. A SAR image is created by transmitting the consecutive pulses of the radio wave to illuminate the target area, in which by the receiver antenna, the radio wave bounced back off a target on the ground is then received and recorded. In comparison, the SAR sensor is more adaptable than the optic sensor. The optics sensor depends more on the weather condition and daylight state. Meanwhile, the SAR sensor can possibly be demonstrated in any condition. Since the SAR signal is able to easily penetrate rain, mist, clouds and fog with very little attenuation, it allows the operation in any weather conditions [1]. Moreover, the SAR sensor is very compact and portable. Therefore, SAR can be implemented in many applications, for example: satellite [2], airborne SAR [3], UAV SAR [4], tactical aircraft SAR [5] and balloon SAR [6]. Thus, SAR technologies attract more responsiveness.

Since 2007, the Josapahat Microwave Remote Sensing Laboratory (JMRSL), Centre of Environmental and Remote Sensing (CEReS), Chiba University has been conducting research and development on some projects related to the application and technologies of SAR. Some examples of those projects are GAIAII/LAPAN-Chiba satellite, JX-II UAV SAR and Airborne SAR for Boeing 737. Therefore, the development of a reliable SAR system is crucial. The critical part of the SAR system is the antenna system which has the function as a SAR sensor in which the antenna is functioned as a spearhead for the SAR system. Hence, good SAR data can possibly be produced by nothing but good

Received 29 August 2017, Accepted 31 October 2017, Scheduled 20 November 2017

* Corresponding author: Farohaji Kurniawan (farohaji.kurniawan@lapan.go.id; farohaji@gmail.com).

[1] Josaphat Microwave Remote Sensing Laboratory, Center for Environmental Remote Sensing Graduate School Advanced Integration Science, Chiba University, Chiba, Japan. [2] Center for Aeronautics Technology, National Institute of Aeronautics and Space, Bogor, Indonesia. [3] Research Center for Frontier Medical Engineering, Inage, Chiba University, Japan. [4] School of Engineering and Digital Arts, University of Kent, Canterbury CT2 7NT, United Kingdom.

antennas bearing both good receiver and transmitter. Thus, an investigation of the characteristics of the single patch antenna is necessary.

In this paper, a single patch X-band circularly polarized SAR (CP-SAR) antenna is presented. The Circularly Polarized (CP) type is chosen due to the benefit of the CP. The CP antenna is more adaptable to the Faraday Effect than the Linier Polarization (LP) type [7]. In addition, the signal degradation might occur due to the atmospheric environments, but the CP antenna is more unaffected to it. Moreover, modern SAR systems have implemented the CP-SAR type in many fields such as in military [8], disaster monitoring [9], and agriculture [10]. Furthermore, the CP antenna type acts very resiliently to the polarization type. Thus, the CP is able to receive and also transmit signal in any polarizations, vertical, horizontal, or CP.

The proposed antenna is printed on a substrate with the dielectric constant of 2.17 and thickness of 1.6 mm, while the mid-band frequency is at 9.4 GHz. The simulation has produced a good result with the impedance bandwidth of 27% (8.2 GHz–10.76 GHz), while the bandwidth of the axial ration is obtained on 10.3% (8.85 GHz–9.83 GHz), and the gain of the antenna is up to 6.7 dBic in the centre of the frequency. The minimum requirements of the antenna design are shown in Table 1.

Table 1. The specification of the antenna.

	Parameter	**Value**
Electrical	Frequency (GHz)	9.0–9.8
	VSWR	≤ 2
	Polarization (T_x/R_x)	circular
	Axial ratio (dB)	≤ 3
	Return loss (dB)	≥ 10
	Gain (dBic)	≥ 5
Mechanical	Weight (kg)	< 0.4
	Thickness (mm)	< 10
Environmental	Temperature (°C)	-50 to $+55$
	Operating altitude (km)	550–800
	Vibration (g rms)	14

2. DETAIL DESIGN OF THE ANTENNA

The antenna is printed in double substrates. The patch antenna functions as a radiator of the antenna set in the front layer, with the feed line design set on the backside of the first substrate, and then the ground-plane set on the second substrate. The patch antenna is designed with circular shape, and the radius of the patch is $r = 4.925$ mm, then the length and width of the patch antenna are represented, $l = 32.0125$ mm. In the middle of the patch antenna lies the square-shaped slot. Then a pair of square shapes set on 45° to y-axis and $-45°$ to x-axis function as truncation factors. Truncation's factor design is represented by W_t and L_t, $W_t = 2.8$ mm as the width of the truncation shape and $L_t = 3$ mm as the depth of the truncation's shaped. The dimension of the feeding line is represented by $W_f = 4.05$ mm, $W_{f1} = 1.35$ mm, $W_{f2} = 2.025$ mm, $W_{fh} = 2$ mm, $L_{f1} = 8$ mm, $L_{f2} = 10$ mm, $L_{f3} = 12.5$ mm, and $L_{f4} = 14.5$ mm. The detailed geometry design of the antenna is shown in Figure 1.

2.1. Design of Circular-Ring-Slot on Ground-plane

The proposed design of the antenna is in the form of a circle-shaped patch with the truncation and a small square one functioned as a slot set in the centre of the patch. The unique part of this design lies in the CRS on the ground-plane which is combined with the square slot in the centre patch having the function of enhancing the bandwidth. This antenna is designed with double layers. The front layer is set as a radiation patch, and then the feeding line set on the backside of the front layer. The backside of the bottom layer is used as the place for the ground plane, and on that ground plane it is functioned

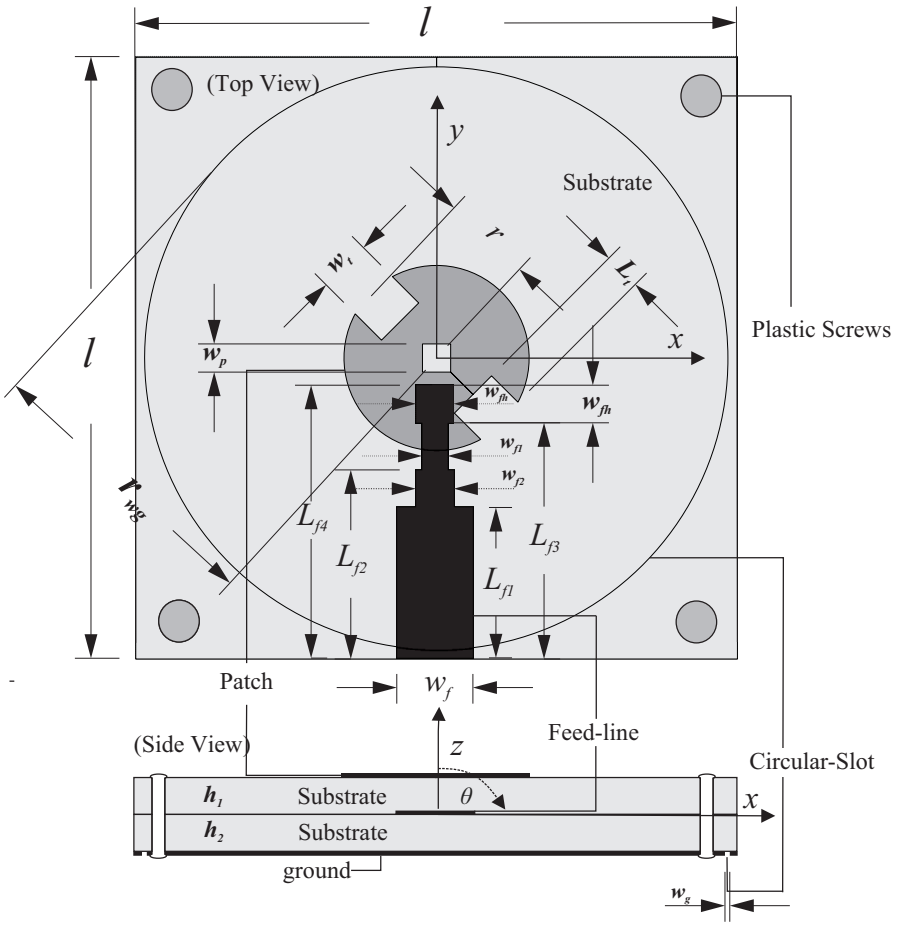

Figure 1. Detail design of the antenna.

as a place of the CRS. The antenna design is etched on the substrate with dielectric constant of 2.17, thickness h of 1.6 mm and loss of tangent of 0.0005.

2.1.1. The Circular-Ring-Slot Geometry

Many methods are applied to enhance the impedance bandwidth, AR bandwidth and gain, for example, slot microstrip antenna [11–13], gain enhancement with air gap and foam [14–17], and bandwidth improvement using metamaterial [18]. In this design, CRS on the ground slot and square slot on the patch of antenna are proposed to enhance the impedance bandwidth, AR bandwidth and gain. To complete the investigation, the variety of design of the circular slot on the ground plane is presented in this section.

The ground-plane is designed with four models. The design of model 1 has the widest CRS among others. The width of the circular slot of model 1 is $R_w = 1$ mm which is represented with $R_1 = 14.5$ mm and $R_2 = 15.5$ mm. Then, the CRS of model 2 is constructed with $R_1 = 15.4$ mm and $R_2 = 15.5$ mm, which means that the width of R_w is 0.1 mm. The CRS of model 3 is the smaller among the others, with $R_1 = 13.5$ mm and $R_2 = 13.3$ mm. The last improvement for ground plane is the plain ground plane without the CRS. Figure 2 shows the designs of the CRS on the ground plane.

2.1.2. Effect of the Circular-Ring-Slot

The characteristics of the current distribution are as shown in Figure 3. Figure 3(a) shows the current distribution of ground-plane model 1 which becomes the widest CRS design. The antenna design is simulated by giving the waveguide port at the edge of the feeding line. The current flows through the

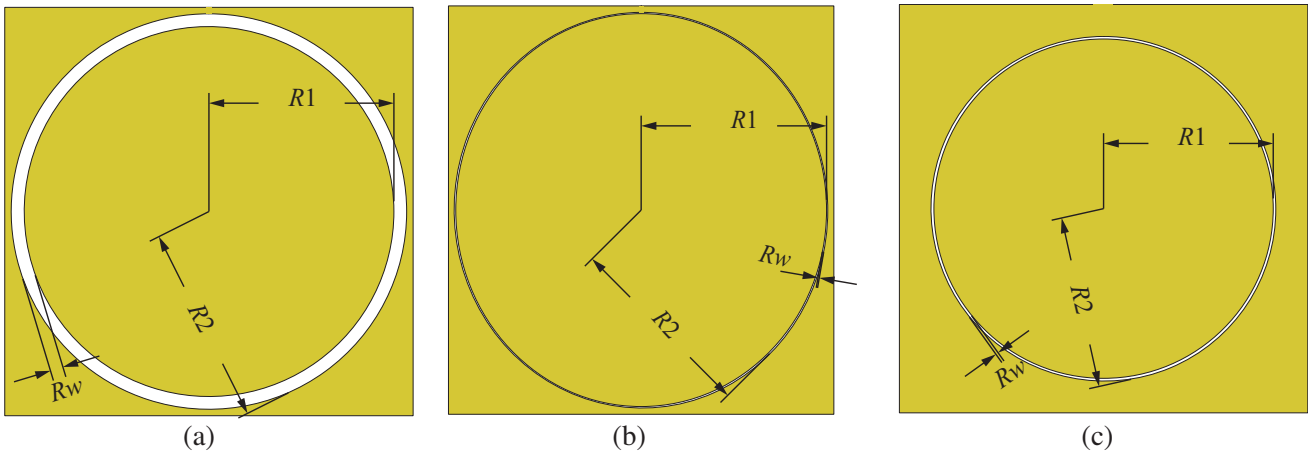

Figure 2. Design of circular-ring-slot (CRS). (a) Model 1. (b) Model 2. (c) Model 3.

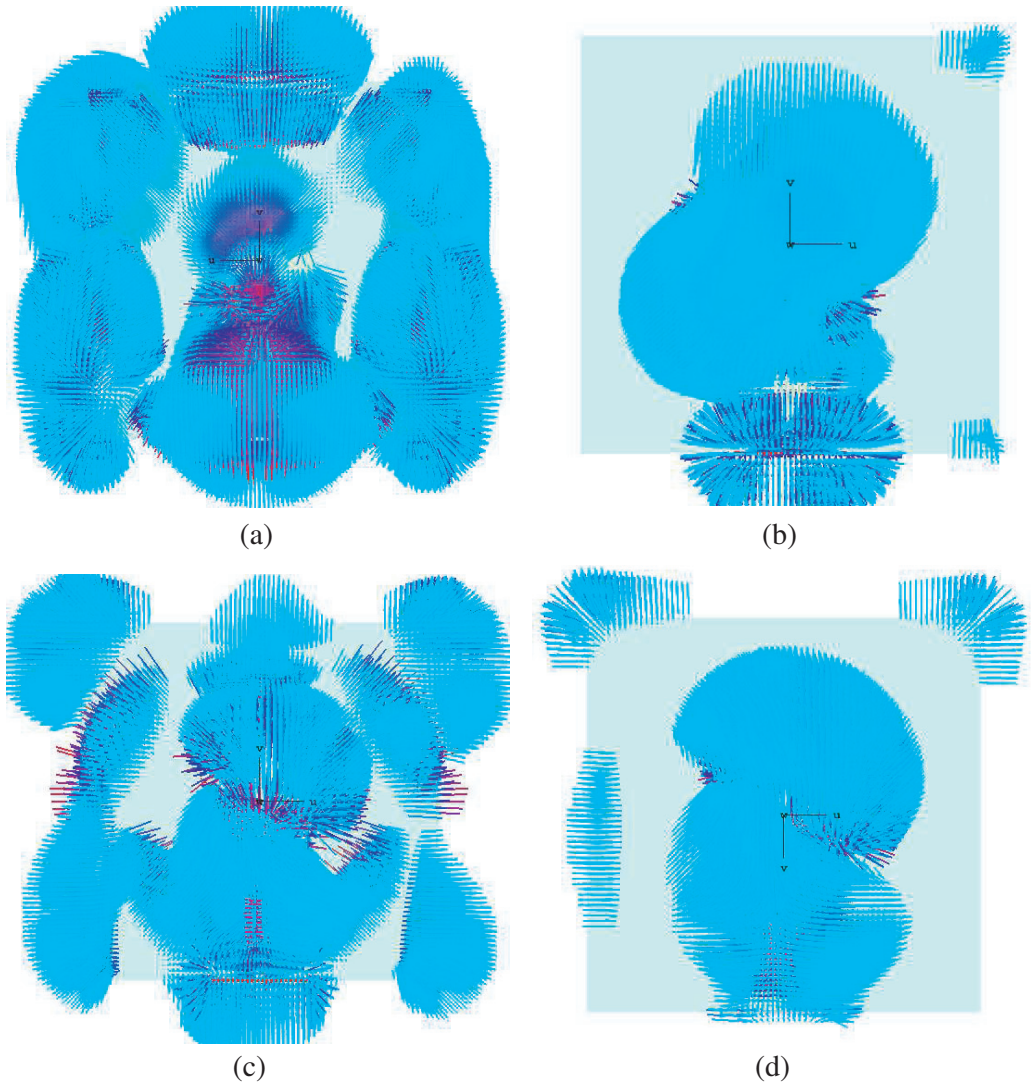

Figure 3. Current distribution. (a) Ground-plane model 1. (b) Ground-plane model 2. (c) Ground-plane model 3. (d) Ground-plane model 4.

feeding line towards the patch-shaped one, then this patch acts as the radiator of the antenna. Later on, the current is spreading on the patch radiator to make a wave rotation. Nonetheless, this circular motion of the current is not strong enough, thus the AR cannot yield less than 3 dB. In this model, the CRS creates a gap of the cooper on the ground-plane and then continues in the current tracing of the slot in a circular movement. The current is stuck at this CRS and creates a boundary.

Figure 3(b) shows the current distribution of the ground-plane model 2. The current flows from the bottom of the feeding line to the center of the antenna. Then, it is distributed to the patch radiator. Evidently, it shows the current distribution which circulates to the left-hand side. Afterward, Figure 3(c) shows the current distribution of the ground-plane model 3. The current's flow starts from the feeding line. Then, the current spread is more evenly distributed across the surface, and its case is similar to model 1. The ground-plane model 4 shown in Figure 3(d) shows the ground-plane design for model 4 which is designed without any slot. The purpose of the design is investigating the diversity of the characteristics of the antenna as it is set either with or without a slot. The characteristic of the current distribution of ground-plane model 4 is similar to that of the ground-plane of model 2.

Evidently, the CRS design has some influences on the characteristics of the antenna. In Figure 4(a), it presents the simulation result of the reflection coefficient, S_{11} by varied CRS on the ground-plane. The CRS model 1 is formed by $R_1 = 14.5$ and $R_2 = 15.5$ mm. Thus, the width of the CRS is R_w 1 mm. This model can produce the bandwidth of reflection coefficient, and $S11$ is up to 23.73% (10.1 GHz–12.33 GHz). However, the simulated result in the centre of frequency is shifted to 11.15 GHz and the deepest curve at 11.68 GHz which is obtained at −38.08 dB. By setting R_1 to 15.4 mm, the bandwidth of the reflection coefficient S_{11} is 27% (8.2 GHz–10.76 GHz). Then, at the resonant frequency of 9.4 GHz it achieves −22.4 dB. A smaller CRS is implemented in the next simulation, with $R_1 = 13.5$ mm and $R_w = 13.5$ mm. Thus, the width of the CRS (R_w) is 0.2 mm. Ground-plane model 3 can produce the bandwidth of the reflection coefficient S_{11} with 0.98% (10.62 GHz–11.60 GHz). The last model for this ground-plane investigation is the one designed without a slot. This model can obtain the bandwidth of reflection coefficient S_{11} up to 36.48% (8.5 GHz–11.90 GHz). Nonetheless, the simulation result of the ground-plane model 4 is not too deep, and it tends to be declivous. Based on the result of the simulation, the performance is shown by the ground-plane model 2.

Figure 4(b) shows the comparison of the simulated AR by varying the width of CRS. The ground-plane model 1 can achieve merely 2.6% (10.27 GHz–10.52 GHz). This result is shifted from the requirement of the center frequency of 10.40 GHz up to 0.60 dB. Furthermore, the ARBW for this model is unacceptable. When $R_w = 0.1$ mm, the ARBW can obtain 12.7% (8.8 GHz–9.84 GHz) and then at the the center frequency of 9.4 GHz yield 0.62 dB. The simulated result of ground-plane model 2 is acceptable and satisfying. The ground-plane model 3 with $R_w = 0.2$ mm cannot be obtained under 3 dB. The last model is ground-plane model 4 which is constructed without the CRS. From this model, the ARBW can obtain 7% (9.15 GHz–9.85 GHz), with the deepest curve at 9.45 GHz which yields 0.12 dB. The result of model 4 is good enough. Nevertheless, it is unacceptable because the reflection coefficient,

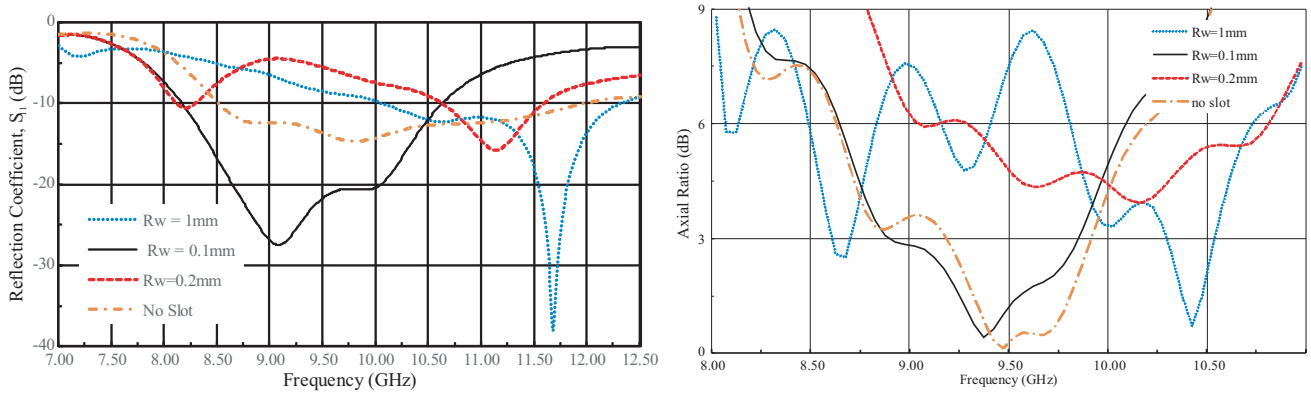

Figure 4. Effect of the CRS. (a) Reflection coefficient, S_{11}. (b) Axial ratio.

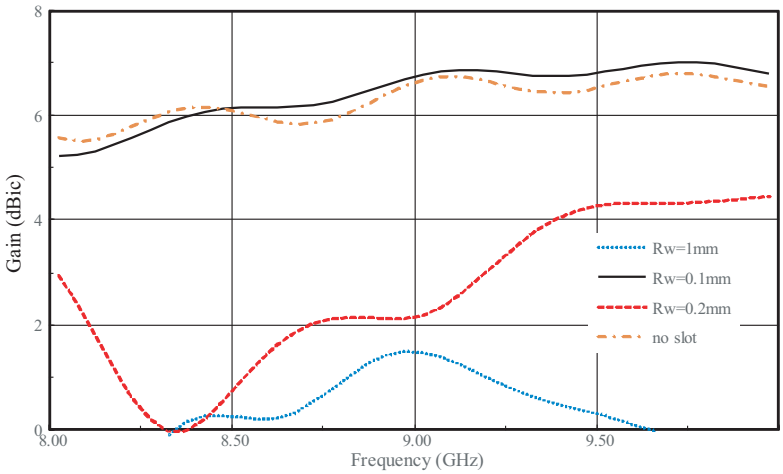

Figure 5. Simulated result of gain.

Table 2. Performance of the antenna design with CRS variation.

Model	Width of CRS (mm)	Impedance bandwidth (GHz)	3 dB ARBW (dB), %	Gain (dBic)
Ground-plane model 1	1	10.1–12.33, 23.73%	10.27–10.52, 2.6%	0.5 to 1.5
Ground-plane model 2	0.1	8.2–10.76, 27%	8.8–9.85, 10.6%	6.67 to 6.81
Ground-plane model 3	0.2	10.62–11.60, 0.98%	none	2.12 to 4.36
Conventional model	Without CRS	8.5–11.90, 36.48%	9.15–9.85, 7%	6.79 to 7.03

S_{11}, is nothing but 0.7 GHz.

The comparison of the simulated gain by variation of the CRS is shown in Figure 5. The result for ground-plane model 4 shows that the gain for ground-plane model 4 cannot achieve a good result. As a result, the ground plane model 2 can obtain about 6.7 dBic. At 9 GHz, it yields 6.79 dBic; at 9.8 GHz it yields 6.99 GHz; at the centre frequency 9.4 GHz, it obtains 6.74 dBic. In the ground-plane model 3, it yields 4.36 dBic, then 4.13 dBic in the center frequency. The last variation of the ground-plane model 4 is the one designed without a CRS, from which it has then found that the simulated gain achieves a good result of up to 6.44 dBic in the center frequency. At 9 GHz, it obtains 6.67 dBic, and at the high frequency 9.8 GHz it obtains 6.75 GHz. The conclusion for the comparison of the simulated gain is that the best performance for the gain is the ground-plane model with $R_w = 0.1$ mm. The detailed conclusion is presented in Table 2.

2.2. Bandwidth Enhancement with Slot on the Centre Patch

In this antenna design, the widening bandwidth is implemented by two factors; firstly by using the Circular-Ring-Slot (CRS) on the ground-plane and secondly by implementing a shape slot in the centre patch of the antenna. The design of the CRS is already explained in the previous section. Figure 6 shows the comparison of the model designs with slot of different shapes .

To complete the investigation of the antenna design, the patch model design is varied into 5 models. The first model of the slot is a small square-shaped one by the width of 1.5 mm. Then, the second patch model for this antenna is the one with ellipse shape. This ellipse slot is represented by the 0.75 mm as a width and 1.5 mm as a length. The next simulation is by giving a conventional design to the antenna, which is the one without a slot on the patch. A circle-shaped slot is also implemented in the antenna design, and its radius is 0.75 mm. The last modification is by changing the slot of the patch to a big square shape with the width of 3 mm.

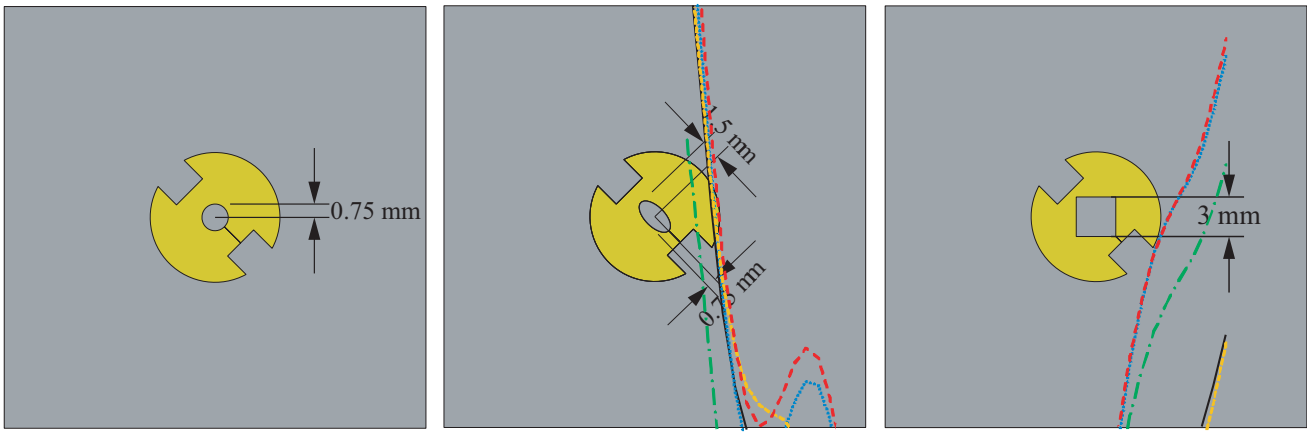

Figure 6. Design patch radiator with slot shaped. (a) Circular slot. (b) Ellipse slot. (c) Big squared slot.

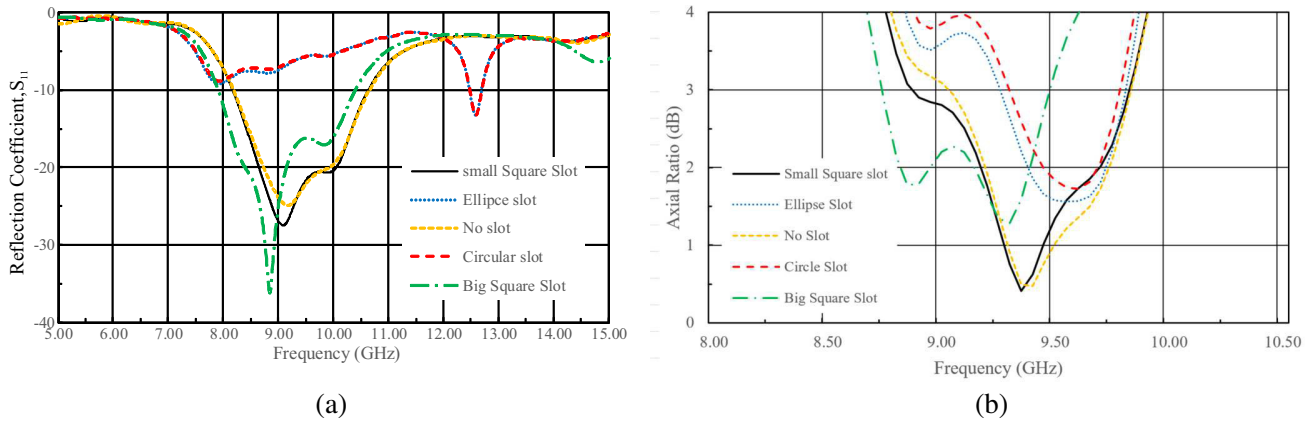

Figure 7. Effect of the CRS. (a) Reflection coefficient, S_{11}. (b) Axial ratio.

The aim of this study focused in this section is to investigate the feasibility of the diversity of the result by concentrating more on the model variety of differently shaped slots on the patch. In general, all of the slot models can produce decent gain at about 6 dBic. Figure 7 shows the simulated impedance bandwidth of the varieties of slot shapes. The characteristics of the reflection coefficients, S_{11}, of ellipse

Table 3. Slot shaped observation result.

Model	Deepest point of IMBW (dB), GHz	Impedance bandwidth (GHz)	3 dB ARBW (dB), %	Deepest point of ARBW (dB), GHz
Square-slot	−27.46, 9.1	8.2–10. 76, 27%	8.85–9.85, 10.6%	0.41, 9.35
Ellipse-Slot	−13.23, 12.6	12.5–12.7, 2.12%	9.25–9.8, 5.8%	1.56, 9.55
conventional model	−25.6, 9.3	8.2–10.2, 21.7%	9.05–9.86, 8.6%	0.47, 9.4
Circular-slot	−13.23, 12.6	12.5–12.7, 2.12%	9.3–9.75, 4.7%	1.73, 9.6
Big-Square-Slot	−35.71, 8.9	7.9–10.4, 26.6%	8.75–9.5, 8%	1.28, 9.3

slot are similar to that of the small square slot. The low frequency and high frequency are exactly in the same place at 8.2 GHz to 10.76 GHz of about 27%. The only thing which makes both characteristics of the reflection coefficient, S_{11}, different is the depth of the curve of the graphic. The detailed conclusion of the slot-shape observation is presented in Table 3.

3. FABRICATION AND MEASUREMENT RESULT

To prove a reliable design of the antenna, the fabrication and measurement have to be conducted to verify the simulated result. In this case, the circumspection is required to produce a precise antenna and a good measurement result. The antenna design has a total dimension of 32 mm × 32 mm × 3.2 mm. Figure 8 shows the fabricated antenna.

Figure 9(a) depicts the comparison of the circular polarization performance of measured and simulated experimentations. The results have a good agreement in which the measurement result can produce the ARBW of 1.03 GHz or equal to 10.95% (8.83 GHz–9.86 GHz), and at the same time the deepest point of curve at 9.17 GHz is 0.38 dB. Furthermore, the center-frequency of 9.4 GHz yields

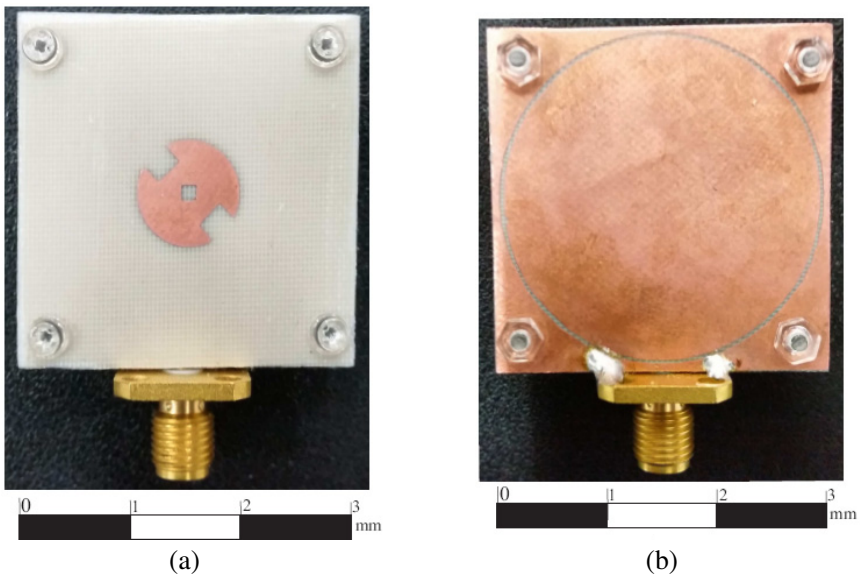

Figure 8. Fabricated antenna. (a) Patch of the antenna. (b) Ground-plane of the antenna.

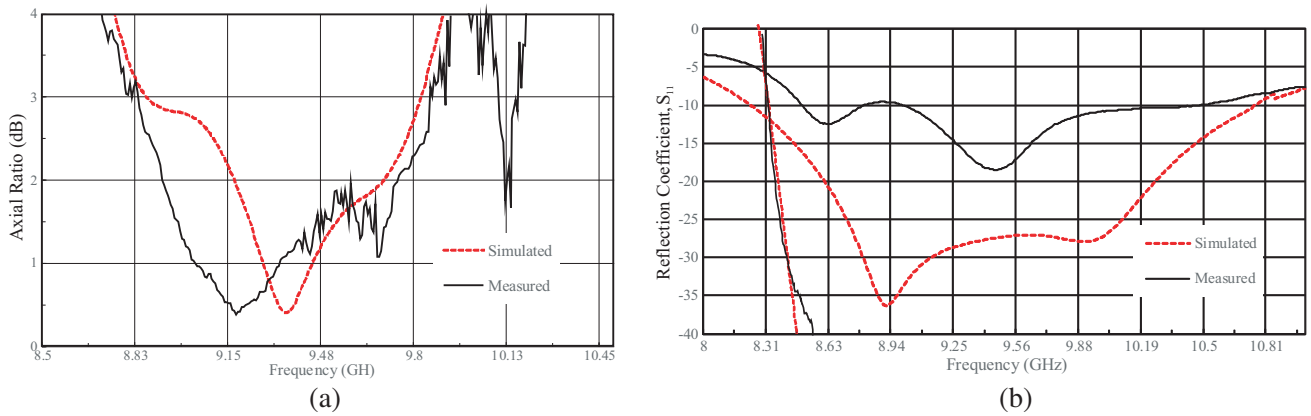

Figure 9. (a) Axial ratio simulated result against measured result. (b) Reflection coefficient, S_{11} simulated result against measured result.

1.28 dB of AR. Meanwhile, the simulated experimentation can produce AR with the bandwidth of 0.97 GHz or equal to 10.3% (8.86 GHz–9.83 GHz), and the deepest point of curve at 9.34 GHz is 0.43 dB and at the resonant frequency of 0.63 dB. The simulated and measured results meet the suitability.

The minimum requirement of the bandwidth of the reflection coefficient S_{11} under -10 dB is 0.8 GHz. As shown in Figure 9(b), the simulation and measurement can produce acceptable results compared to the minimum requirement. The impedance bandwidth is up to 1.51 GHz or equal to 16% (8.9 GHz–10.41 GHz) of the measurement. At the centre frequency, the measured result is up

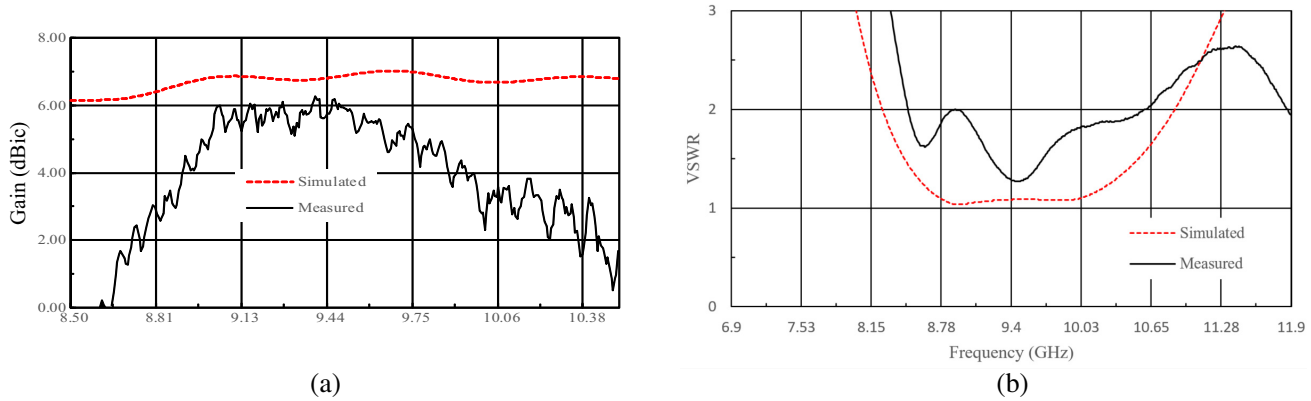

Figure 10. (a) Simulated and measured gain of proposed antenna. (b) Simulated and Measured VSWR.

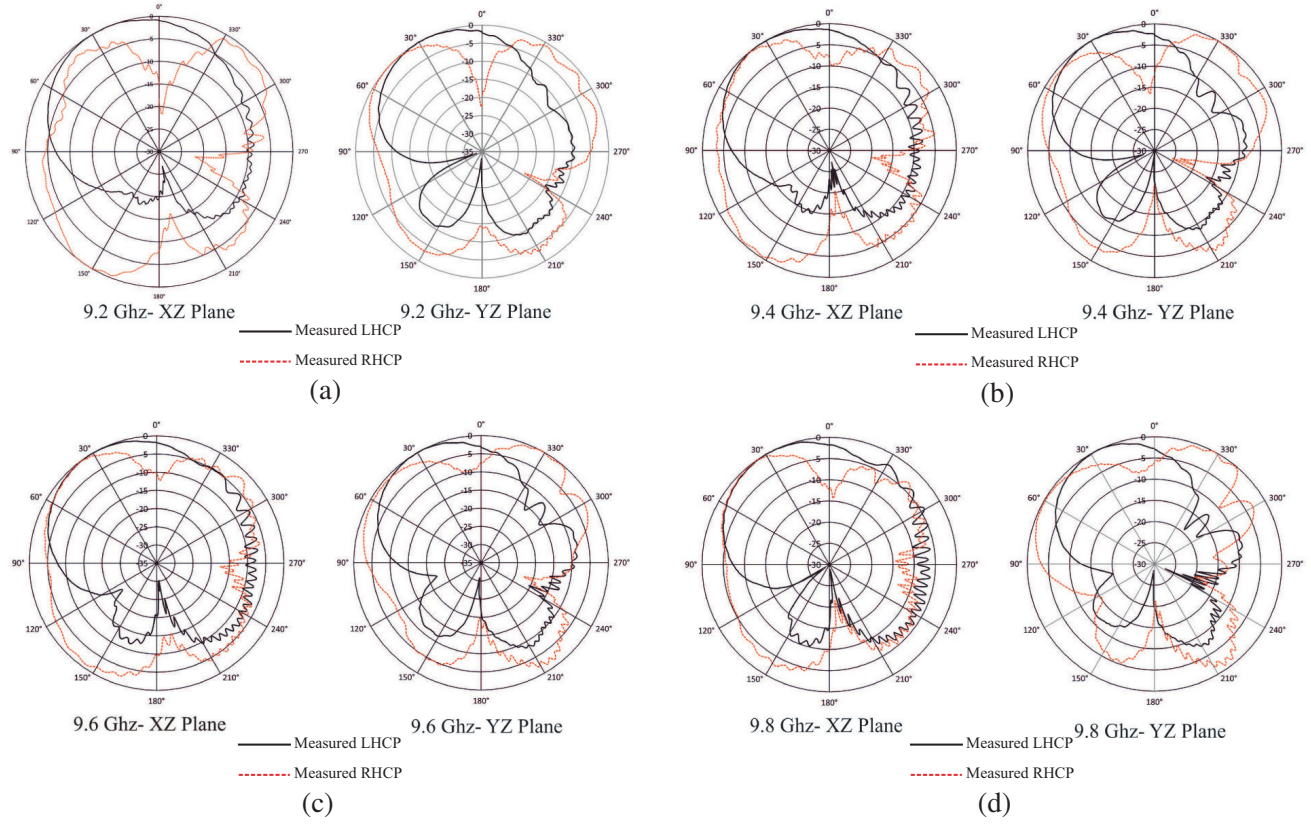

Figure 11. Measured and simulated radiation pattern of proposed X-band antenna: (a) 9.2 GHz; (b) 9.4 GHz; (c) 9.6 GHz; (d) 9.8 GHz.

to −18.19 dB, while the deepest curve is at 9.46 GHz of 18.48 dB. However, this measurement result decreases compared to the simulated one. The impedance bandwidth of the measurement yields 2.56 GHz or 27% (8.2 GHz–10.76 GHz), −27.7 dB of the centre frequency, and the deepest point of curve is at 8.91 GHz up to −36.36 dB.

Figure 10(a) highlights the simulated and measured gains. The minimum requirement of gain of the antenna design is approximately 5 dBic. The results of simulation and measurement meet the minimum requirement. The simulation can achieve a quite good result, which is about 7.4 dBic at the resonant frequency, 6.81 dBic at the lower frequency and 6.69 dBic at the higher frequency. On the other hand, the measured result shows a reduction; however it remains an acceptable one. In the lower frequency, it yields 5.3 dBic, while in the higher frequency it is 4.91 dBic, and this point (9.8 GHz-higher frequency) also becomes the lower point of gain. However, this result is still acceptable due to the average value of the measured gain at desired frequency of about 5.6 dBic to the minimum requirement of the antenna design.

The result for VSWR also shows the indication of good agreement as depicted in Figure 10(b). This is an indication that the simulated and measured results are acceptable to < 2 in the desired frequency. The average value of simulated result is 1.07 and 1.5 for the measured result. Figure 11 shows the LHCP against the RHCP radiation pattern in the X-Z plane and Y-Z plane at four discrete frequencies; 9.2 GHz, 9.4 GHz, 9.6 GHz and 9.8 GHz.

4. CONCLUSION

CRS has managed to enhance the performance of the reflection coefficient and the ARBW, and it also produces a good gain. Evidently, ground-plane model 2 with 0.1 mm CRS can enhance the impedance bandwidth under −10 dB of 27% and at 3-dB which obtains 12.7 dB and the gain up to 6.7 dBic. A small square slot with the diameter of 1.5 mm is suitable for the proposed antenna. It can produce the impedance bandwidth under −10 dB of 27%. The effect of 1.5 square slot can reach minimum requirement of the impedance bandwidth, and it has a good agreement with the minimum requirement. It can produce the impedance bandwidth up to 16% and 3-dB ARBW obtaining 10.95%. It shows a slightly low result compared to the simulated one; however, it is still considered as an acceptable one. The imprecise measured result is due to fabrication errors (drilling, cutting, soldering and etching). To sum it up, this novel antenna design has a good performance.

ACKNOWLEDGMENT

This research is supported in parts by the Japan Science and Technology Agency (JST) Japan International Cooperation Agency (JICA) FY2010-2016 Science and Technology Research Partnership for Sustainable Development (SATREPS); the European Space Agency (ESA) Earth Observation Category 1 under Grant 6613; the 4th Japan Aerospace Exploration Agency (JAXA) ALOS Research Announcement under Grant 1024; the 6th JAXA ALOS Research Announcement under Grant 3170; the Japanese Government National Budget Ministry of Education and Technology (MEXT) FY2015-2017 under Grant 2101; Chiba University Strategic Priority Research Promotion Program FY2016-FY2018; Taiwan National Space Organization (NSPO) under Grant NSPIO-S-105096; and Indonesian National Institute of Aeronautics and Space (LAPAN); National Institute for Environmental Studies (NIES) for ASTER images; GSI for GPS ground measurement data.

REFERENCES

1. Ulaby, F. T., R. K. Moore, and A. K. Fung, *Microwave Remote Sensing: Active and Passive, Vol. I*, Artech House, Norwood, 1981.
2. James, Y. Y., et al., "An X-band SAR satellite payload design with low cost approach for disasters management," *2015 IEEE 5th APSAR*, 15568731, 2015.
3. Natele. A., P. Berardino, C. Esposito, and S. Perna, "Airborne SAR for high resolution imaging," *2017 Joint Urban Remote Sensing Event (JURSE)*, 16868028, 2017.

4. Sri Sumantyo, J. T., "Development of circularly polarized Synthetic Aperture Radar onboard Unmanned Aerial Vehicle (CP-SAR UAV)," *2012 IEEE IGARSS*, 13133238, 2012.
5. Wang, N., Y. Li, Y. Bu, and J. Chen, "SAR sensor employment planning for tactical aircraft," *2010 The 2nd ICCAE*, 11259605, 2010.
6. Yang, H., L. Teng, Y. Huang, J. Yang, and X. Yang, "Multi-spotlight balloon SAR: An interesting microwave remote sensing mission for distributed monitoring," *2013 IEEE IGARSS*, 14059446, 2014.
7. Osanai, Y., J. T. Sri Sumantyo, and Z. Baharuddin, "Development of spaceborne antenna for circularly polarized SAR using Kevlar honeycomb core," *2015 IEEE 5th Asia-Pacific Conference on APSAR*, 15558266, 2015.
8. Anter, Y. M., M. A. Henry, and G. C. McCormick, "Circular polarization for remote sensing of precipitation: Polarization diversity work at the National Research Council of Canada," *IEEE Antennas and Propagation Magazine*, Vol. 34, No. 6, 1345–1354, 1989.
9. Sri Sumantyo, J. T., H. Wakabayashi, A. Iwasaki, F. Takahashi, H. Ohmae, H. Watanabe, R. Tateishi, F. Nishio, M. Baharuddin, and P. R. Akbar, "Development of circularly polarized synthetic aperture radar onboard microsatellite (muSAT CP-SAR)," *PIERS Proceedings*, 382–385, Beijing, China, Mar. 23–27, 2009.
10. Sri Sumantyo, J. T., "Development of Circularly Polarized Synthetic Aperture Radar (CP-SAR) onboard small satellite," *PIERS Proceedings*, 334–341, Marrakesh, Morocco, Mar. 20–23, 2011.
11. Kurniawan, F., J. T. Sri Sumantyo, G. S. Prabowo, and A. Munir, "Wide bandwidth left-handed circularly polarized printed antenna with crescent slot," *2017 Progress In Electromagnetics Research Symposium (PIERS)*, 1047–1050, St Petersburg, Russia, May 22–25, 2017.
12. Ghali, H. A. and T. A. Moselhy, "Broad-banda and cirularly polarized space-filling-based slot antennas," *IEEE Transactions on Microwave Theory and Techniques*, Vol. 53, No. 6, Jun. 2005.
13. Taher, H. and R. Farrell, "Broadband high gain SIW cavity square slot antenna for X-band applications," *Antennas and Propagation Conference (LAPC), Loughborough*, 2016.
14. Jamlos, M. F., T. Bin Abdul Rahman, M. R. Kamarudin, M. T. Ali, M. Nor Md Tan, and P. Saad, "The gain effects of air gap quadratic aperture-coupled microstrip antenna array," *PIERS Proceedings*, 462–465, Cambridge, USA, Jul. 5–8, 2010.
15. Ali, M. T., H. Jaafar, S. Subahir, and A. L. Yusof, "Gain enhancement of air substrates at 5.8 GHz for microstrip antenna array," *Electromagnetic Compatibility*, Vol. 18, No. 1, 477–480, 2012.
16. Raut, R. and K. Talandage, "Bandwidth and gain enhancement of rectangular MSA by using parasitic patch and capacitive feeding technique for wideband application," *International Conference on Microwave, Optical and Communcation Engineering*, IIT Bhubaneswar, India, Dec. 2015.
17. Ta, S. X. and T. K. Nguyuen, "AR bandwidth and gain enhancements of patch antenna using single dielectric superstrate," *IEEE Electronics Letters*, Vol. 53, No. 15, 2017.
18. Dai, Y. L., et al., "A novel compact ultra-wideband metamaterial-based microstrip antenna," *IMWS-AMP*, 2016.